Editors' Suggestion

Strength of Mechanical Memories is Maximal at the Yield Point of a Soft Glass

Srimayee Mukherji,[1,*] Neelima Kandula,[1] A. K. Sood,[2,3] and Rajesh Ganapathy[3,4,†]
[1]Chemistry and Physics of Materials Unit, Jawaharlal Nehru Centre for Advanced Scientific Research, Jakkur, Bangalore 560064, India
[2]Department of Physics, Indian Institute of Science, Bangalore 560012, India
[3]International Centre for Materials Science, Jawaharlal Nehru Centre for Advanced Scientific Research, Jakkur, Bangalore 560064, India
[4]School of Advanced Materials, Jawaharlal Nehru Centre for Advanced Scientific Research, Jakkur, Bangalore 560064, India

(Received 26 August 2018; published 16 April 2019)

We show experimentally that both single and multiple mechanical memories can be encoded in an amorphous bubble raft, a prototypical soft glass, subject to an oscillatory strain. In line with recent numerical results, we find that multiple memories can be formed sans external noise. By systematically investigating memory formation for a range of training strain amplitudes spanning yield, we find clear signatures of memory even beyond yielding. Most strikingly, the extent to which the system recollects memory is largest for training amplitudes near the yield strain and is a direct consequence of the spatial extent over which the system reorganizes during the encoding process. Our study further suggests that the evolution of force networks on training plays a decisive role in memory formation in jammed packings.

DOI: 10.1103/PhysRevLett.122.158001

In a seminal experiment, Paulsen *et al.* observed that the addition of noise helped form memories of multiple strain amplitudes in a periodically sheared dilute non-Brownian suspension [1]. This phenomenon, first predicted numerically [2], shares striking similarities with findings on charge density wave solids [3] and helps distinguish this class of memory from other well-known memory effects [4,5]. Subsequently, simulations found encoding of multiple mechanical memories possible even in amorphous solids subject to a cyclic shear. In amorphous solids, however, the source of noise is intrinsic as opposed to hydrodynamic [1] and stems from the complexity of the energy landscape [6]. The ability to form such memories highlights the interplay between noise and the underlying reversibility-irreversibility transition (RIT) at a threshold strain amplitude γ_c in these systems [7–9]. The yielding transition in amorphous solids, under oscillatory shear, shares qualitative features with RIT, and γ_c has been identified with the yield strain γ_y [9–12]. In the absence of noise, repeated cycles of training at an amplitude of $\gamma_t < \gamma_c$ eventually result in the system reaching a reversible steady state. Since reversibility at γ_t implies reversibility for all $\gamma < \gamma_t$, even when trained at multiple amplitudes $\gamma_1, \gamma_2, \ldots, \gamma_n$, with $\gamma_1 < \ldots < \gamma_n < \gamma_t$, memory of only γ_t is retained in the steady state. With noise present, the system meanders around a subset of accessible metastable states, and this allows encoding of multiple memories [2,3]. Memory of γ_t(s) can be retrieved by performing a strain sweep and, if present, manifests itself as cusp(s) in irreversibility as $\gamma_\circ$ is swept past γ_t(s). Even while one expects at least a partial retention of the training in the fluctuating steady state [13], evidence for memory for $\gamma_t > \gamma_y$ is currently lacking even in simulations on amorphous solids. Probing memory effects across the yielding transition in soft glasses becomes particularly relevant, given that local plastic rearrangements in these systems are correlated through long-range elastic interactions [11,14–18]. This is unlike sheared dilute suspensions, where particle reorganization events are purely local [8]. Nevertheless, experiments are yet to find signatures of even single memories, let alone multiple ones, and that too below γ_y in amorphous solids.

In this Letter, we study memory formation in a model athermal amorphous solid—bubble rafts [15,19–23]—subject to a cyclic shear. We provide the first experimental evidence of both single and multiple memories in a soft glass. We find the degree to which the system recollects memory of the training is maximal for $\gamma_t \approx \gamma_y$ and is a direct consequence of the large scale spatial reorganization of the system that occurs for training amplitudes in the vicinity of yield.

Our amorphous rafts, a bidisperse mixture of bubbles of diameters of $\sigma_s = 1.1$ mm and $\sigma_l = 1.4$ mm, were formed in a wide-gap circular Couette cell with an inner disk of radius $R_i = 3.1$ cm and an outer cylinder of radius $R_o = 7.5$ cm [Fig. 1(a), Supplemental Material and Fig. S1 [24]]. The inner disk was coupled to a rheometer (MCR 301, Anton-Paar, Austria) for applying precise mechanical forcing. High-speed imaging (Photron Fastcam SA4, Photron, United Kingdom) of the rafts during rheological measurements allowed simultaneous quantification

of single-particle dynamics. We measured the yield point of the bubble raft [Fig. 1(a)] by applying an oscillatory strain, $\gamma(t) = \gamma_\circ \sin(\omega t)$, keeping the angular frequency fixed at $\omega = 0.628$ rad/s and sweeping the strain amplitude $\gamma_\circ$. Figure 1(b) shows the elastic and viscous moduli, G' (black circles) and G'' (red squares), respectively, versus $\gamma_\circ$. The observed behavior is typical of a soft amorphous solid with $G' > G''$ in the linear response regime [28]. The onset of plasticity is characterized by the breakdown of linearity and is followed by a crossover of G' and G'' at $\gamma_\circ = 0.06$, which we identified with γ_y.

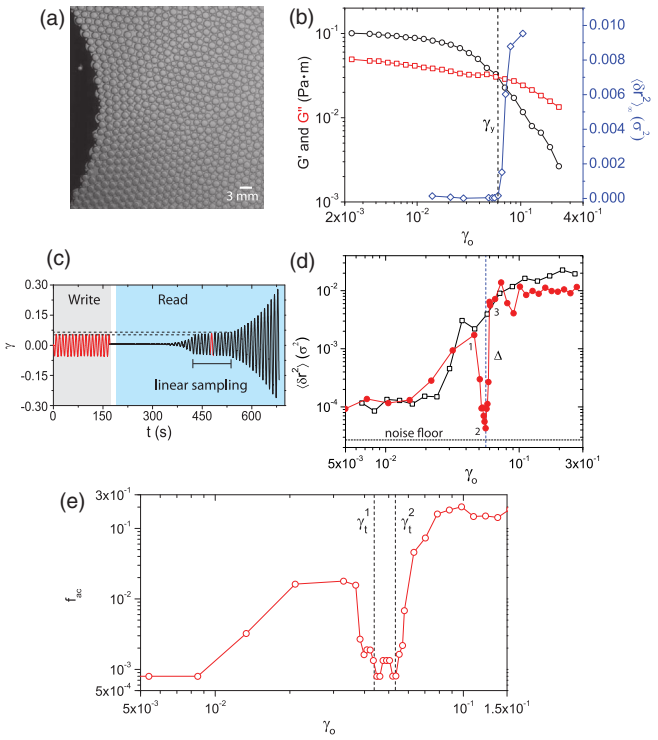

FIG. 1. (a) Snapshot of bubble raft. Ratio of number of small bubbles N_S to large bubbles N_L is $N_S/N_L \approx 1.9$. (b) Amplitude sweep measurements to quantify the yield point γ_y. Elastic and viscous moduli, G' (black circles) and G'' (red squares), respectively, versus amplitude of cyclic shear, $\gamma_\circ$. Vertical line is drawn at $\gamma_y = 0.06$. The variances in particle positions attained at steady state on writing memory, $\langle \delta r^2 \rangle_\infty$ (Supplemental Material, Fig. S2 [24]), are shown as blue diamonds. (c) Typical write and read protocol followed in our experiments. Data correspond to training at strain amplitude of $\gamma_t = 0.056$. Writing is done for $n = 17$ cycles. Memory was read (blue-shaded region) after a 10 s pause after writing (white-shaded region). (d) Evolution of the variance in particle positions $\langle \delta r^2 \rangle$ during read for the untrained system (black squares) and for training at $\gamma_t = 0.056$ (red circles). The horizontal dashed line represents the average noise floor in our experiments (Supplemental Material, Sec. C). (e) Multiple memories: The fraction of active particles, f_{ac} (i.e., fraction of particles with $\langle \delta r^2 \rangle > 0.1\sigma$), versus $\gamma_\circ$ during read, showing two drops at $\gamma_\circ \approx 0.042$ and $\gamma_\circ \approx 0.053$. Multiple memories were more evident in f_{ac} (in the Supplemental Material, Fig. S6 shows signatures of multiple memories in $\langle \delta r^2 \rangle$ [24]).

Recent studies hint of an intimate link between memory formation and RIT [1,2,6], and we confirmed the existence of this transition for our system. The rafts were subjected to repeated strain oscillations $\gamma(t) = \gamma_t \sin(\omega t)$, where $\omega = 0.628$ rad/s (Supplemental Material, Movie S1 [24]) and we quantified the irreversibility in the system with the oscillation cycle number, n. We defined irreversibility as the variance in particle positions, $\langle \delta r^2 \rangle = (1/N) \sum_{i=1}^{N} \delta r_i^2$, between images pertaining to the beginning and end of a strain cycle, i.e., stroboscopic snapshots. Here, $\langle\rangle$ denotes an average over all N particles in the field of view with $\delta r_i = r_i(n) - r_i(n-1)$ being the displacement of particle i, measured stroboscopically, in the nth oscillation cycle. We observed that, for $\gamma_t \leq \gamma_y$, $\langle \delta r^2 \rangle$ dropped to zero with n, whereas for $\gamma_t > \gamma_y$, $\langle \delta r^2 \rangle$, it plateaued at a finite value (Supplemental Material, Fig. S2 [24]). Although experiments and simulations on dilute non-Brownian suspensions observed that a large n (typically > 100) was needed to reach steady state, we found $n \approx 7$–10 cycles in our study, which is consistent with previous experimental observations on athermal dense amorphous solids [29]. The steady-state value of the variance $\langle \delta r^2 \rangle_\infty$—the order parameter for the transition —shows that the RIT for bubble rafts is centered at γ_y [blue diamonds in Fig. 1(b)] [9,11].

Besides confirming the existence of a RIT, the above experiments (Supplemental Material, Fig. S2 [24]) also helped train the raft at various γ_t's (Supplemental Material, Movie S2 [24]). After training, we performed a "read" comprising a sequence of systematically increasing oscillatory strain amplitudes, $\gamma_\circ$, spanning γ_t [Fig. 1(c)]. $\gamma_\circ$ was sampled logarithmically far away from γ_t and linearly in its vicinity to better detect memory. To quantify memory, we calculated $\langle \delta r^2 \rangle$ as in write but with one minor difference. Here, $\langle \delta r^2 \rangle = (1/N) \sum_{i=1}^{N} (r_i(\gamma_\circ + \delta\gamma_\circ) - r_i(\gamma_\circ))^2$, where $\delta\gamma_\circ$ is the increment in the read strain amplitude between successive cycles. Figure 1(d) shows $\langle \delta r^2 \rangle$ versus $\gamma_\circ$ for an untrained raft (black squares) and for the same raft trained at $\gamma_t = 0.056$ (red circles). The data were smoothened using a sliding three-point averaging procedure. Although substantial irreversibility was present for $\gamma_\circ < \gamma_t$, the raft retained information of the training (Supplemental Material, Movie S3 [24]), with $\langle \delta r^2 \rangle$ dropping by nearly two orders of magnitude when $\gamma_\circ \approx 0.056$. We ensured that our results were not sensitive to the specific read procedure followed (Supplementary Material Sec. E and Supplementary Material Figs. S3 and S4 [24]). Our findings are consistent with numerical studies in which the trajectory of the system in the potential energy landscape during read showed a closed orbit only for $\gamma_\circ = \gamma_t$, whereas for $\gamma_\circ \neq \gamma_t$, the orbits were open, resulting in $\langle \delta r^2 \rangle > 0$ [6]. Information of the training is also seen as a stress drop when $\gamma_\circ \approx \gamma_t$ in the bulk rheological data (Supplemental Material, Fig. S5 [24]).

The lack of an ordering of reversible states in our rafts, $\langle \delta r^2 \rangle > 0$ for $\gamma_\circ < \gamma_t$, opens up the possibility of encoding of multiple memories without external noise (as in [6]). We trained the raft at two amplitudes, $\gamma_1 = 0.042$ and $\gamma_2 = 0.053$, at once. The "write" comprised 11 oscillation cycles of γ_2 and 22 oscillation cycles of γ_1, and this sequence was repeated twice. Figure 1(e) shows the fraction of active particles, $f_{\rm ac}$, versus $\gamma_\circ$ during the read (Supplemental Material, Fig. S6 [24]). Particles were denoted active if $\sqrt{\delta r_i^2} > 0.1\sigma$ with $\sigma = (\sigma_s + \sigma_l)/2$. Memory of both training amplitudes is evident.

Next, we quantified the formation of single memories for various γ_t's spanning γ_y. Two features in the representative read profiles shown in Fig. 2(a) stand out. First, we observe memory for $\gamma_t > \gamma_y$. This is not entirely surprising because, even under overdriving ($\gamma_t > \gamma_y$), although the system settles down to a fluctuating steady state, there is still a substantial drop in irreversibility during the initial few cycles of training, leaving a partial imprint of γ_t (Supplemental Material, Fig. S2 [24]). The second striking feature is that the magnitude of the drop in $\langle \delta r^2 \rangle$ near γ_t, which is a measure of how well the system retains information of the training, is largest for $\gamma_t = \gamma_y$. We parametrized the strength of memory by Δ, defined as the ratio of $\langle \delta r^2 \rangle$ s of the untrained raft and the trained one at $\gamma_\circ = \gamma_t$ [Fig. 1(d)]. Although some scatter is present, the nonmonotonicity in Δ with γ_t with a maximum at γ_y is indisputable [filled circles in Fig. 2(b)].

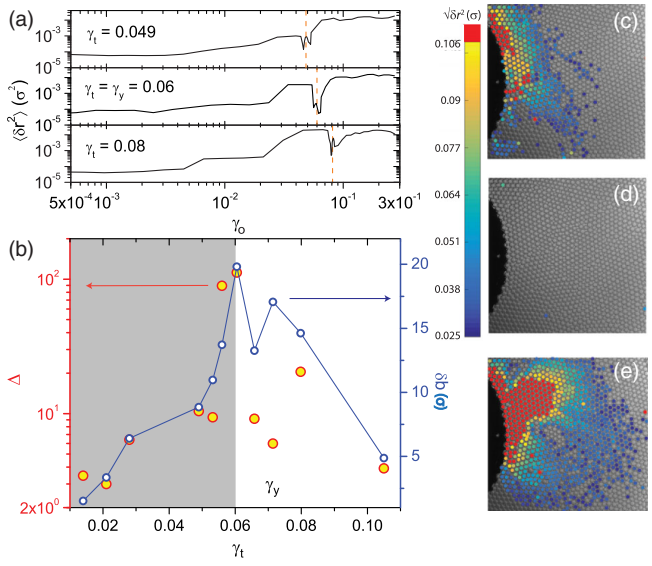

FIG. 2. (a) Representative read profiles for γ_ts across γ_y. (b) Strength of memory, Δ [Fig. 1(d), defined as the ratio of $\langle \delta r^2 \rangle$ of the untrained to the trained raft at $\gamma_\circ = \gamma_t$], versus γ_t (filled red circles). Width of the active region δb shown by hollow blue circles. Preyield regime is shaded gray. (c)–(e) Stroboscopic images of the raft during read, corresponding to points labeled 1 (onset of drop in $\langle \delta r^2 \rangle$), 2 (minimum in $\langle \delta r^2 \rangle$), and 3 (onset of second plateau in $\langle \delta r^2 \rangle$) in Fig. 1(d), respectively. Particles are color coded according to the magnitudes of their displacements.

We gleaned insights into this behavior by quantifying the spatial distribution of irreversible particles during read. Figures 2(c)–2(e) show stroboscopic images of the raft corresponding to read strains labeled 1, 2, and 3 in Fig. 1(d), with the particles color coded according to the magnitudes of their displacements. For $\gamma_\circ$'s straddling γ_t (labeled 1 and 3), particles that underwent substantial irreversible displacement form a reasonably well-defined band adjacent to the inner rotating disk. In the Supplemental Material, Movie S4 [24] shows that, as $\gamma_\circ$ is increased towards γ_t, the width of this band grows radially outwards from the inner rotating disk, collapses when $\gamma_\circ \approx \gamma_t$, and grows radially outwards again as $\gamma_\circ$ is further increased. Next, we measured the distance the edge of the activity field moves, δb, during read for various γ_t's. Here, δb is the difference in the spatial width of the irreversible particle band measured at the onset of the drop and at the minimum in $\langle \delta r^2 \rangle$, respectively; and it corresponds to points labeled 1 and 2 in Fig. 1(d) for $\gamma_t = 0.056$. The trend in δb mimics the one observed in Δ [blue circles in Fig. 2(b)].

Why is there a maximum in Δ *at* $\gamma_t = \gamma_y$? The extent to which the system retains memory of the input depends on how well this information was encoded during training. In the Supplemental Material, Movie S5 [24] shows the spatial evolution of irreversibility for $\gamma_t = 0.056 \approx \gamma_y$. The magnitude of particle irreversibility decays radially from the inner rotating disk and, with increasing n, the width of this activity field decreases and vanishes completely by the end of training. In our wide-gap Couette geometry, the stress decays as $1/r^2$ at a radial distance r from the center of the inner disk [15,22,23]. This stress inhomogeneity results in a curvilinear strain-rate, $\dot{\gamma}$, profile across the gap. To calculate $\dot{\gamma}(r)$, we divided the gap into rings of width 1.22σ, concentric with the inner disk, and then computed the average azimuthal velocity $v(r)$ of the particles within each ring from subsequent images. $v(r)$ was averaged over the first 10 image pairs, corresponding to 0.17 s, of the strain oscillation cycle, wherein the acceleration of the inner disk is almost zero. In the Supplemental Material, Fig. S7 [24] shows the velocity profiles for various γ_t's. We smoothened the velocity profiles to calculate $\dot{\gamma}(r) = (dv/dr) - (v/r)$. Figure 3(a) shows $\dot{\gamma}(r)$ versus r/R_i for a few representative γ_ts spanning yield. The decay in $\dot{\gamma}(r)$ with r implies that, for a given γ_t, bubbles located farther away from the inner disk experience an increasingly smaller fraction of the applied strain rate (also the strain). These regions thus reach a reversible state in fewer training cycles than regions closer to the inner disk, and the edge of the activity field moves towards smaller r/R_i with n (Supplemental Material, Movie S5 [24]).

We quantified the spatial evolution of activity during training by measuring $f_{\rm ac}$ within each ring. Figures 3(b)

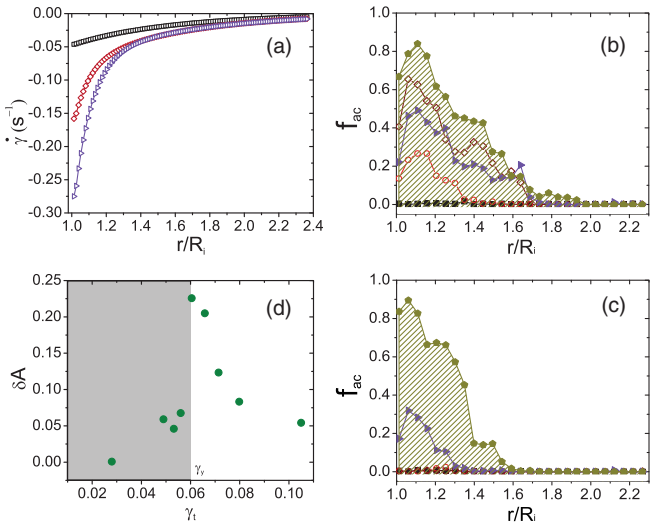

FIG. 3. (a) Strain rate $\dot{\gamma}$ as a function of r/R_i for $\gamma_t = 0.028$ (black squares), $\gamma_t = \gamma_y = 0.060$ (wine-red diamonds), and $\gamma_t = 0.071$ (violet right triangles). r is the distance from the center of the inner moving plate, and R_i is the radius of the inner rotating disk. (b) and (c) f_{ac} as a function of r/R_i for the 2nd and the 16th training cycles, respectively. $\gamma_t = 0.028$ (black squares), $\gamma_t = 0.049$ (red hollow circles), $\gamma_t = \gamma_y = 0.060$ (wine-red open diamonds), $\gamma_t = 0.071$ (violet right triangles), and $\gamma_t = 0.105$ (pale-green pentagons). (d) δA versus γ_t.

and 3(c) show f_{ac} versus r/R_i, for various γ_t's at the beginning and end of the training, respectively. When $\gamma_t \ll \gamma_y$, the strain amplitude is too weak to cause substantial irreversible rearrangements and the final particle packing at the end of training is not very different from the one at the start [red circles in Figs. 3(b) and 3(c)]. Since a sizable fraction of the system is unable to reconfigure, Δ is small. For $\gamma_t \gg \gamma_y$, the strain amplitude is large enough to cause considerable irreversible rearrangements at the beginning of the training, but significant irreversibility also remains at the end, i.e., in the fluctuating steady state [pale-green symbols in Figs. 3(b) and 3(c)]. Thus, Δ is again small. For $\gamma_t \approx \gamma_y$, the edge of the activity field sweeps the largest area between the beginning and end of training, resulting in maximal reconfiguration of the system and a large Δ [wine-red diamonds in Figs. 3(b) and 3(c)]. Mimicking Δ, the area swept between the beginning and end of training δA is nonmonotonic with γ_t, with a maximum at γ_y [Fig. 3(d)]. A previous study on amorphous bubble rafts under nearly identical experimental conditions found a "flow cooperativity length" finite only in the jammed state that resulted in strong nonlocal effects during flow [15]. Such effects are compounded by the presence of a stress inhomogeneity [14], as in our study. Furthermore, experiments on colloidal glasses have shown that spatially cooperative relaxation dynamics is maximal in the vicinity of yield [11]. Whether such spatial correlations have a bearing on the observed maximum in Δ remains to be seen.

We return to our observation of a finite irreversibility for $\gamma_\circ < \gamma_t$ during read. Unlike memory formation in non-Brownian suspensions, where adding noise results in $\langle \delta r^2 \rangle > 0$ for $\gamma_\circ < \gamma_t$ during read [1,2], in jammed packings like ours, it remains unclear. Below, we provide a plausible explanation. Studies on cyclically sheared dense packings find that the fraction of nearest-neighbor contacts broken, f_b, peaks during strain reversal [30]. On training at a given γ_t, however, f_b drops and reaches a steady state, suggesting that the same links are broken during subsequent strain cycles. The contact network that points predominantly along the compression axis cannot remain identical immediately after strain reversal [Fig. 4(a)] [31]. The particle configuration therefore retraces a different path after strain reversal; albeit, this path closes in on itself after a full cycle for $\gamma_\circ = \gamma_t$ and is consistent with $\langle \delta r^2 \rangle \approx 0$ [6]. f_b for any $\gamma_\circ \neq \gamma_t$ during read will not have reached a steady state [30], and the particle packing should essentially behave like an untrained one (open orbits and $\langle \delta r^2 \rangle > 0$). Indeed, we find that $\langle \delta r^2 \rangle$ for the untrained raft (black symbols) almost follows the trained one (red symbols) until the point labeled 1 in Fig. 1(d). Figure 4(b) shows the particle displacement map during read at $\gamma_\circ = 0.073$, which is the equivalent of the point labeled 1 for $\gamma_t = 0.079$. The spatial extent of irreversible displacements looks similar to that after the first cycle of write for $\gamma_t = 0.071$, which is the γ_t closest to $\gamma_\circ = 0.073$ in our study [Fig. 4(c)]. Perhaps the most intriguing finding, which our study does not answer, is how the raft manages to retain memory of γ_t in spite of behaving like an untrained one close to γ_t.

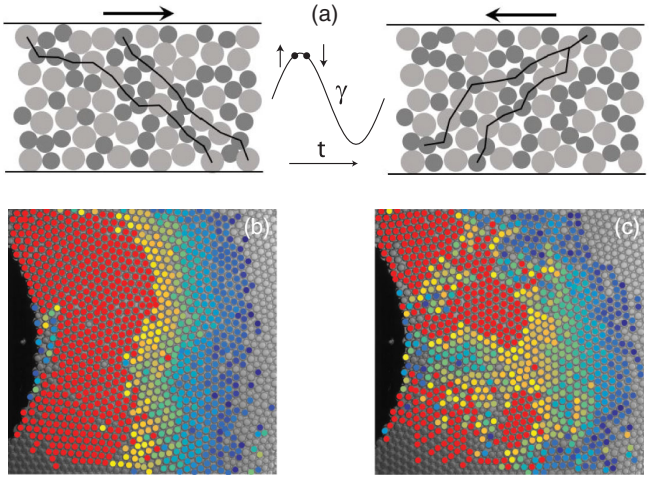

FIG. 4. (a) Schematic of force chains in jammed packings immediately after strain reversal. Although the particle configuration remains identical after reversal, the contact network is not. (b) Particle displacement map for $\gamma_\circ = 0.073$ during read. This strain corresponds to the maximum before the drop (equivalent of point labeled 1) for a $\gamma_t = 0.079$. (c) Particle displacement map after the first cycle of write for $\gamma_t = 0.071$, which is closest to point 1 in our study.

Collectively, our study provides the first direct experimental evidence of both single and multiple mechanical memories in athermal amorphous solids under cyclic shear. Remarkably, the strength of single memories is maximal near γ_y and is intimately connected to the extent to which particle irreversibility spatially evolves during training. This suggests that the recent observations of growing spatial correlations in the vicinity of the yielding transition [11,18] may have a direct role in the formation of mechanical memories. Given that numerical studies find cyclic shear to be a potential route to prepare well-annealed glasses [32], it is tempting to wonder if the strength of memory formation can be used as readout for ultrastability. A natural step forward would be to explore connections between memory formation and the evolution of force networks with training. We believe that frictionless athermal systems like dense assemblies of bubble rafts and emulsions, where force chains can be quantified through shape distortions [33–36], will prove to be ideal platforms for these measurements.

A. K. S thanks Dept. of Sci. and Tech. (DST), Govt. of India for a Year of Science Fellowship. R. G. thanks International Centre for Materials Science & School of Advanced Materials, JNCASR for support.

*Corresponding author.
mou2792@gmail.com
†Corresponding author.
rajeshg@jncasr.ac.in

[1] J. D. Paulsen, N. C. Keim, and S. R. Nagel, Phys. Rev. Lett. **113**, 068301 (2014).
[2] N. C. Keim and S. R. Nagel, Phys. Rev. Lett. **107**, 010603 (2011).
[3] M. L. Povinelli, S. N. Coppersmith, L. P. Kadanoff, S. R. Nagel, and S. C. Venkataramani, Phys. Rev. E **59**, 4970 (1999).
[4] K. Jonason, E. Vincent, J. Hammann, J. P. Bouchaud, and P. Nordblad, Phys. Rev. Lett. **81**, 3243 (1998).
[5] J. P. Sethna, K. Dahmen, S. Kartha, J. A. Krumhansl, B. W. Roberts, and J. D. Shore, Phys. Rev. Lett. **70**, 3347 (1993).
[6] D. Fiocco, G. Foffi, and S. Sastry, Phys. Rev. Lett. **112**, 025702 (2014).
[7] D. J. Pine, J. P. Gollub, J. F. Brady, and A. M. Leshansky, Nature (London) **438**, 997 (2005).
[8] L. Corte, P. M. Chaikin, J. P. Gollub, and D. J. Pine, Nat. Phys. **4**, 420 (2008).
[9] D. Fiocco, G. Foffi, and S. Sastry, Phys. Rev. E **88**, 020301 (R) (2013).
[10] I. Regev, T. Lookman, and C. Reichhardt, Phys. Rev. E **88**, 062401 (2013).
[11] K. Hima Nagamanasa, S. Gokhale, A. K. Sood, and R. Ganapathy, Phys. Rev. E **89**, 062308 (2014).
[12] I. Regev, J. Weber, C. Reichhardt, K. A. Dahmen, and T. Lookman, Nat. Commun. **6**, 8805 (2015); N. C. Keim and P. E. Arratia, Soft Matter **9**, 6222 (2013); E. D. Knowlton, D. J. Pine, and L. Cipelletti, Soft Matter **10**, 6931 (2014).
[13] N. C. Keim, J. D. Paulsen, and S. R. Nagel, Phys. Rev. E **88**, 032306 (2013).
[14] J. Goyon, A. Colin, G. Ovarlez, A. Ajdari, and L. Bocquet, Nature (London) **454**, 84 (2008).
[15] G. Katgert, B. P. Tighe, M. E. Möbius, and M. van Hecke, Europhys. Lett. **90**, 54002 (2010).
[16] P. Schall, D. A. Weitz, and F. Spaepen, Science **318**, 1895 (2007).
[17] V. Chikkadi, G. Wegdam, D. Bonn, B. Nienhuis, and P. Schall, Phys. Rev. Lett. **107**, 198303 (2011).
[18] A. Ghosh, Z. Budrikis, V. Chikkadi, A. L. Sellerio, S. Zapperi, and P. Schall, Phys. Rev. Lett. **118**, 148001 (2017).
[19] L. T. Shi and A. S. Argon, Philos. Mag. A **46**, 255 (1982).
[20] W. L. Bragg and J. F. Nye, Proc. R. Soc. London, Ser. A **190**, 474 (1947).
[21] G. Debregeas, H. Tabuteau, and J.-M. di Meglio, Phys. Rev. Lett. **87**, 178305 (2001).
[22] J. Lauridsen, G. Chanan, and M. Dennin, Phys. Rev. Lett. **93**, 018303 (2004).
[23] P. Schall and M. van Hecke, Annu. Rev. Fluid Mech. **42**, 67 (2010).
[24] See Supplemental Material at http://link.aps.org/supplemental/10.1103/PhysRevLett.122.158001 for experimental details and supporting figures, which also includes Refs. [25–27].
[25] G. D. Miles and J. Ross, J. Phys. Chem. **48**, 280 (1944).
[26] A. L. Kuehner, J. Chem. Educ. **35**, 337 (1958).
[27] J. W. McBain and W. C. Sierichs, Journal of the American Oil Chemists' Society **25**, 221 (1948).
[28] P. Sollich, Phys. Rev. E **58**, 738 (1998).
[29] N. C. Keim and P. E. Arratia, Soft Matter **9**, 6222 (2013).
[30] S. Slotterback, M. Mailman, K. Ronaszegi, M. van Hecke, M. Girvan, and W. Losert, Phys. Rev. E **85**, 021309 (2012).
[31] M. L. Falk, M. Toiya, and W. Losert, arXiv:0802.1752v2.
[32] P. Leishangthem, A. D. Parmar, and S. Sastry, Nat. Commun. **8**, 14653 (2017).
[33] J. Brujić, S. F. Edwards, I. Hopkinson, and H. A. Makse, Physica A (Amsterdam) **327**, 201 (2003).
[34] J. Zhou, S. Long, Q. Wang, and A. D. Dinsmore, Science **312**, 1631 (2006).
[35] K. W. Desmond and E. R. Weeks, Phys. Rev. Lett. **115**, 098302 (2015).
[36] R. Höhler and S. Cohen-Addad, Soft Matter **13**, 1371 (2017).